CHAPTER IV
THERMAL AND MECHANICAL PROPERTIES OF PP/ORGANOCLAY NANOCOMPOSITES

4.1 Abstract

PP/organoclay nanocomposites with various clay contents were prepared via a master batch by melt blending in a twin screw extruder using Surlyn® as a reactive compatibilizer. The properties of PP/organoclay nanocomposites, crystal structure, thermal behavior, mechanical properties and oxygen gas permeability, were investigated and compared to pure PP. At a smaller amount of organoclays (1-5 wt%), the degradation temperature at maximum rate of weight loss, as well as the crystalinities, melting and crystallization temperatures of the nanocomposites was greater than pure PP. The mechanical properties were reduced with increasing the clay content. The reduction of mechanical properties may involve with the aggregations of clay or the remaining of some impurities in bentonite. The oxygen gas permeability of the nanocomposite films was decreased when the clay content increases due to the improvement of gas barrier properties of organoclay in nanocomposites.

4.2 Introduction

In recent years, polymer nanocomposites have attracted great interest, both in industry and in academia, because they often exhibit remarkable improvement in materials properties when compared with virgin polymer or conventional micro and macro-composites. These improvements can include high moduli, increased strength and heat resistance, decreased gas permeability and flammability, and increased biodegradability of biodegradable polymers [1].

Nanoclays have further attracted significant amount of interest because of ready availability and their low cost disc-like structure with very high aspect ratio which can maximize the reinforcing. During recent years, bentonites have been investigated in the development of polymer nanocomposites [2, 3]. Bentonite is clay generated from the alternation of volcanic ash, consisting predominantly of montmorillonite. Depending on their genesis, bentonites may contain a variety of accessory minerals such as quartz, feldspar, calcite, gypsum and other metal oxides. The presence of these minerals influences the grade and some properties of bentonite clays.

Polypropylene (PP) is one of the most widely used thermoplastic polymers due to its low price and balanced properties. However, polypropylene is a hydrophobic polymer which is incompatible with hydrophilic clay and hence it is difficult to get the exfoliated and homogeneous dispersion of the clay particles at the nanometer level in the matrix polymer. Normally, there are two ways to compatibilize the hydrophilic clay and hydrophobic PP. One is to organically modify the clay with cationic alkylammonium surfactants via cation exchange reaction [4]. The other way is by using a compatibilizer, such as ethylene methacrylic acid copolymer, Surlyn®. There are two important factors to achieve the exfoliation of the clay layer silicates: (1) the compatibilizer should be miscible with polymer matrix, and (2) it should include a certain amount of polar functional groups in a molecule. Surlyn® can fulfill the two requirements and is frequently used as a compatibilizer for polypropylene nanocomposites [2].

The aim of this study is to prepare PP/organoclay nanocomposites. The properties of these nanocomposites, i.e. crystal structure, thermal behavior, mechanical properties and oxygen gas permeability, with various clay contents were investigated.

4.3 Experimental

A. Materials

Sodium activated bentonite (Na-BTN), under the trade name Mac-Gel® (GRADE SAC), with cationic exchange capacity (CEC) of 44.5 meq/100 g clay, was supplied by Thai Nippon Co., Ltd. Thailand. Dipalmitoylethy hydroxyethylmonium methosulfate was purchased from Sunny World Co., Ltd. Sodium-neutralized ethylene-co-methacrylic acid with MFI = 4 dg/min used as a compatibilizer was purchased from DuPont Co Ltd. Polypropylene (PP) with MFI = 11 dg/min was purchased from Thai Petrochemical Industry Public Co., Ltd (IRPC Co., Ltd). Ethanol (C_2H_5OH) 98% v/v was commercially purchased from Carlo Erba.

B. Preparation of Organo-modified Bentonite

In a container, 350 g of Na-bentonite, Na-BTN, was swollen in 1.05 liters of distilled water for 24 h, followed by heated at 80°C for 30 min. In another container, a cationic surfactant with 2.0 equivalents of CEC was dissolved in 100 ml of ethanol at 80°C for 30 min. After that, the solution of both containers were mixed and vigorously stirred at 80°C for 3 h. The resulting organomodified bentonite, denoted as OBTN was filtered and washed with hot water several times to remove the excess surfactant. Then, it was dried in vacuum oven at 100°C overnight, ground, and screened through a 325 mesh sieve.

C. Preparation of PP/Organo-modified Bentonite Nanocomposite Films

PP/organoclay nanocomposites were prepared by conventional melt intercalation a Collin D-8017 Model T-20 co-rotating twin-screw extruder with L/D=30 and D=25 mm. The operating temperatures of extruder were maintained at 80, 170, 180, 190, 200, and 210 °C from hopper to die respectively. The screw speed was maintained at 50 rpm. The master batches containing 50 wt% organomodified clays with the compatibilizer was added to PP and Surlyn®, fixed at 6 wt%, in appropriate amounts to obtain nominal contents of 1, 3 and 5 wt% clays in the nanocomposites. Each composition was premixed by a tumble mixer for 10 min before introducing into the twin-screw extruder and extruded through a single strand die. The yielded single strands of the PP/clay nanocomposites were obtained and solidified by cool water, palletized and then dried in a vacuum oven at 80°C before characterizations by SEM, TGA, and DSC.

PP and nanocomposite pellets have different thermal history. That is, nanocomposite pellets were prepared by using twin-screw extruder whereas PP pellets were not processed by twin-screw extruder.

The nanocomposites films were prepared by blown film extrusion machine. The nanocomposites pellets were dried in vacuum oven at 80°C for 12 h prior to blowing. Following extrusion conditions were employed, the rotational speed of screw of 50 rpm and blowing ratio of 1.52. The barrel and mold temperature were 210 °C. The thickness of the films was controlled to about 45 μm. The nanocomposite films from blow molding were used for preparing intelligent film and studying mechanical properties.

The nanocomposites films which were prepared by compression molding machine were used to investigate crystal structure and oxygen permeability constants. The thickness of the films was controlled to about 150 μm. The mold containing the pellets was preheated at 200°C for 5 min, followed by compressed under 10 tons of force for 5 min. After that the molding was cooled to 50 °C under pressure.

PP and nanocomposite films have different thermal history. That is, nanocomposite films were prepared by using twin-screw extruder and blow molding or compression molding whereas PP film was only processed by blow molding or compression molding.

D. Characterizations

The X-ray Diffractometer (XRD) was used to determine the interlayer spacing of pristine bentonite, organomodified bentonite, and to observe the crystal structure of nanocomposites. Wide angle ray diffraction-X(WAXD) were patterns obtained by usingdiffrac 2002Rigaku Model Dmax a tofiltered Cu K-meter with Ni_{α} (λ = 0.154 nm) kV and 40tion operated at radia a tube current of 30 mA. The organoclay powder samplesw ere measured in2the θ range of 2degree 20-swith scan For the .degree 0.01min and scan step /degree 2speed nanocomposite ,film samples periment was performed on athe ex2-4degree 0sdegree 5scan speed with smin and / egreed 0.02scan step .

Fourier transform infrared spectroscopy (FT-IR) was used to investigate the presence of the cationic surfactant. The FT-IR spectra were recorded using a Nicolet Nexus 670 FT-IR spectrometer in the frequency range of 4000-400 cm^{-1} with 32 scans at a resolution of 2 cm^{-1}.

Thermogravimetric analysis (TGA) was used to study thermal stability of organomodified bentonite and PP/organoclay nanocomposites as compared to the pure PP.DTA curves-TG ,collected on a Perkin-Elmer Pyris Diamond TG/DTA instrument was carried out from 30°C to 900°C at a heating rate of 10°C/min in a nitrogen atmosphere of 200 ml/min. The degradation temperature, initial degradation temperature, weight loss, and final degradation temperature of the samples were determined. The nanocomposite pellets from twin screw extruder as well as PP pellets were30loaded on the platinum pan and heated from ° C to900°C at a heating rate of 10°flow of $_2$min under N/C 2m 00lmin/.

A Differential Scanning Calorimeter (DSC), Perkin-Elmer DSC 7, was used to measure the crystallization and melting behavior of the PP/organoclay nanocomposites. All operations were performed under a nitrogen atmosphere. The samples were first heated from 30°C to 200°C at a heating rate of 10°C/min in order to eliminate the influence of thermal history and then cooled down at a rate of 10°C/min from 200°C to 30°C to observe the melt crystallization behavior. After that the sample was immediately reheated to 200°C at the same heating rate in order to observe the melting behavior. The crystallinity can be calculated with the following formula

$$\%\ \text{crystallinity} = \frac{\Delta H_{sample}}{\Delta H^0_{PP}} \times 100$$

ΔH_{sample} = enthalpy of fusion of the sample (J/g)

ΔH^0_{PP} = enthalpy of fusion of completely crystalline PP (~ 209 J/g)

A Scanning Electron Microscope (SEM), JEOL (JSM-5800 LV), was used to observe the dispersion of clay particles in the PP matrix. The selected samples, which were nanocomposite pellets from twin screw extruder as well as PP pellets, were dipped and fractured in liquid nitrogen. Then the samples were coated with gold under vacuum to make them electrically conductive before viewing under a scanning electron microscope (SEM) operating at 15 kV.

The mechanical properties of PP/organoclay nanocomposite as well as neat PP films were performed with Lloyd Universal Testing Machine, at room temperature following the procedure described in ASTM D882. The films were prepared by blown film extrusion machine of thickness of 45 μm and were cut in machine direction into rectangular shape with 10x100 mm. The crosshead speed was 50 mm/min and the load cell was 500 N. The values of tensile strength, percentage of elongation at yield and Young's modulus for virgin PP and PP/organoclay nanocomposites were investigated. The results from this test were reported as the average of the data taken from 5 specimens. PP and nanocomposite films have different thermal history. That is, nanocomposite films were prepared by using twin-screw extruder and blow molding whereas PP film was only processed by blow molding.

Gas permeability tester, Oxygen Permeation Analyser Model 8000, Illinois Instrument Inc., was used to determine oxygen permeability constants of pristine PP and nanocomposite films. Gas permeation experiments were investigated following the procedure described in ASTM D1434. The films were prepared from a compression-molded sheet with the same thickness of 150 μm and were cut into circular shape with 15 cm in diameter. The thickness of the films was measured by using the peacock digital thickness gauge model PDN 12N by reading 15 points at random position over tested area and the results were averaged.

4.4 Results and Discussion

A. Characterizations of the Organomodified Bentonite

The X-ray diffraction patterns of Na-bentonite (Na-BTN) and organomodified bentonite (OBTN) are given in Fig. 5.1 (a) and (b), respectively. The (001) diffraction peaks of BTN presents at $2\theta = 7.62°$ and $2\theta = 5.92°$ and 4.42° for OBTN which correspond to the interlayer spacing of 1.15, 1.49 and 1.99 nm, respectively. The interlayer spacing of OBTN is larger than their pristine clays. This evidence indicates that the molecules of alkylammonium surfactant are incorporated between the silicate layers and expanded them.

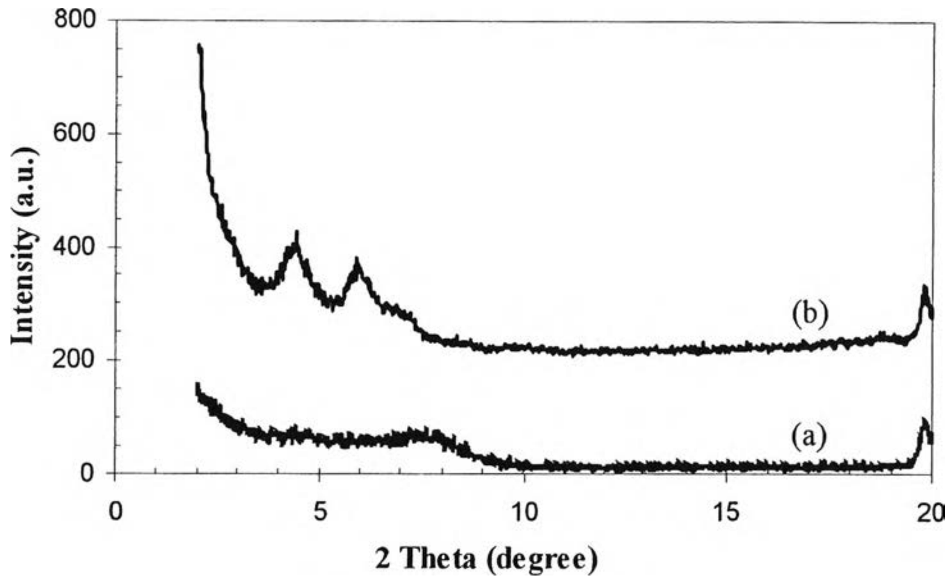

Figure 4.1 The WAXD patterns: (a) Na-BTN and (b) OBTN.

The OBTN was investigated by using FT-IR in order to confirm the incorporation of alkylammonium surfactant molecules between the silicate layers. Fig. 4.2 (a) and (b) shows the FT-IR spectra of Na-BTN and OBTN, respectively. After the modification of BTN, A pair of strong bands 2852 and 2921 cm^{-1} at each spectrum can be assigned to the symmetric and asymmetric stretching vibration of methylene group) of the guest molecules, respectively. The absorption bands at 1740 cm^{-1} is observed due to the stretching vibration of carbonyl group (>C=O). These results support the incorporation of alkylammonium surfactant molecule between the silicate layers [4].

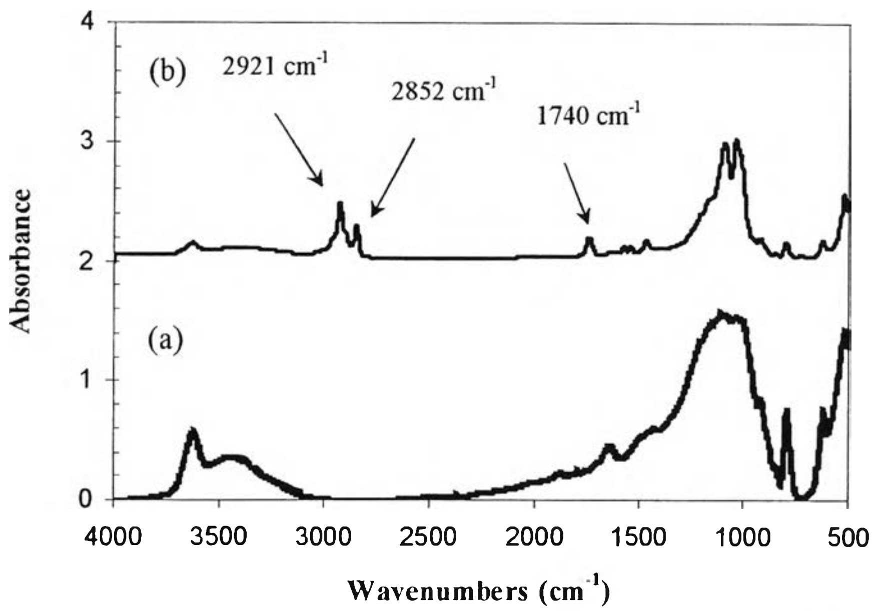

Figure 4.2 FT-IR spectra: (a) Na-BTN and (b) OBTN.

The results of thermogravimetric analysis (TGA) of Na-BTN and OBTN were represented in Table 4.1 and Fig. 4.3. The content of the organic component was determined from the weight loss during TGA. For Na-BTN, the weight loss was observed over temperature range of 44-76 and 617-657 °C, corresponding to the loss of the physically adsorbed water dehydroxylation of clay, respectively. The mass loss of OBTN was investigated in the range 270-370 °C, derived from the decomposition of the intercalated cationic surfactants within the clay interlayer [5, 6].

Table 4.1 Thermal behavior of BTN and OBTN

Sample	Mass Loss H_2O (wt%)	Mass Surfactant (wt%)	Char Residual (wt%)	Desurfactant		
				T_d (°C)	T_i (°C)	T_f (°C)
BTN	0.52	-	98.33	-	-	-
OBTN	0	35.4	64.3	336.8	270.8	367.8

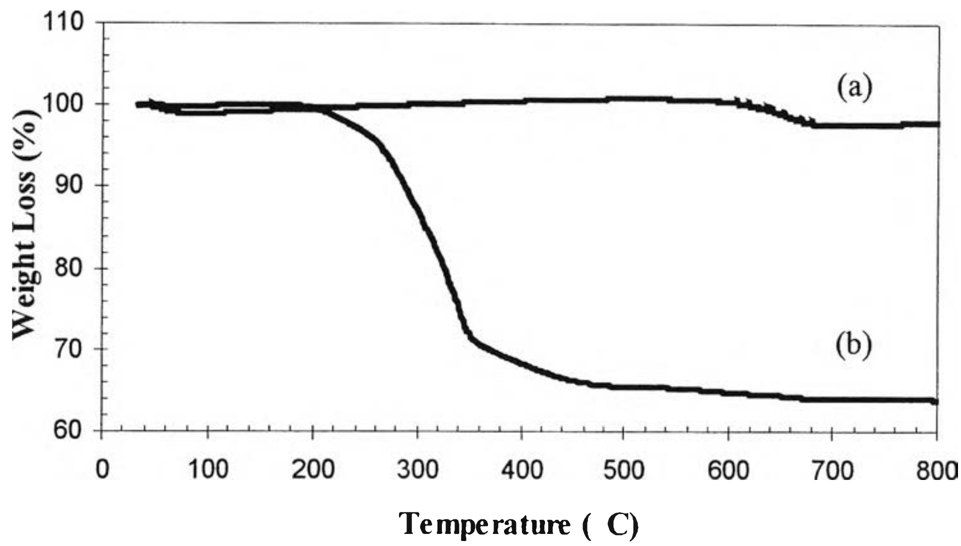

Figure 4.3 Thermal behavior: (a) Na-BTN and (b) OBTN.

B. Crystal Structure of PP/Organoclay Nanocomposites

Crystal structure of the nanocomposites was examined by XRD with the 2θ range of 2-40°, as indicated in Fig. 4.4. According to the WAXD pattern, the (001) diffraction peaks of 3% and 5%clay in nanocomposite films presents at $2\theta = 5.88°$ and $2\theta = 5.72°$ which correspond to the interlayer spacing of 1.50 and 1.54 nm, respectively. Nevertheless, at 1%clay, the low angle peak was not observed. This may imply that some silicate layers were delaminated and dispersed in the PP matrix. Therefore, some exfoliated structure was achieved at 1%clay. From the peak position of α structure, virgin PP reveals five major diffraction peaks at the following 2θ angles: 14.18°, 16.62°, 18.32°, 20.92°, and 21.68° from α crystalline phase: $(110)_{\alpha}$, $(040)_{\alpha}$, $(130)_{\alpha}$ and $(111, 041)_{\alpha}$ crystal planes, respectively. There is no evident difference between pristine PP and nanocomposites in the WAXD pattern, implying that the addition of organoclay does not affect the crystal structure of PP matrix [3, 5, 7].

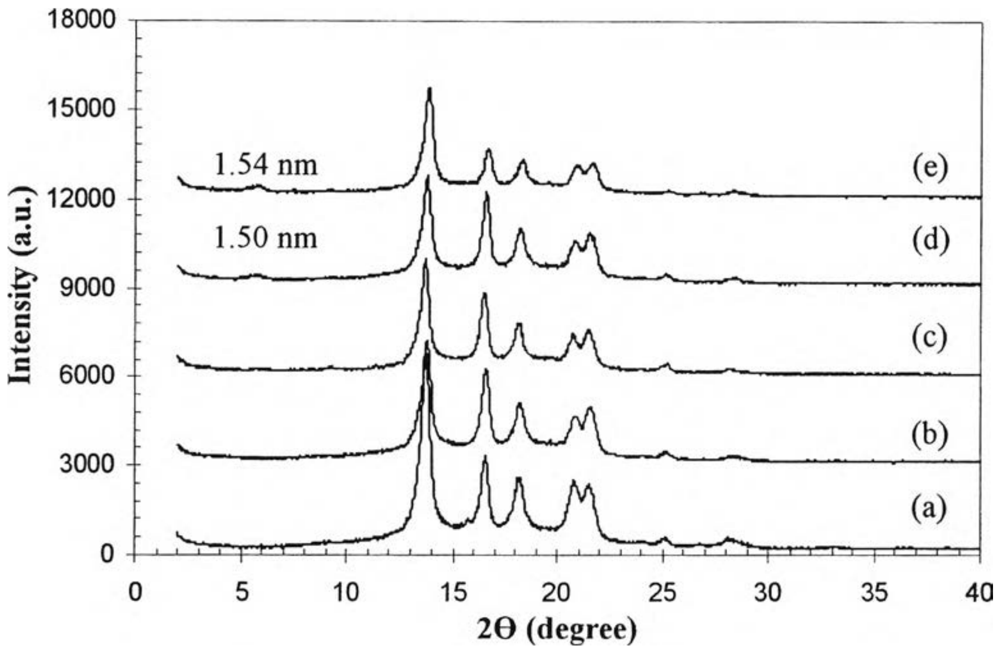

Figure 4.4 The WAXD patterns of PP and PP/organoclay nanocomposites: (a) PP, (b) PP/6%Surlyn, (c) PP/6%Surlyn/1%Clay, (d) PP/6%Surlyn/3%Clay, and (e) PP/6%Surlyn/5%Clay.

C. Thermal Stability of PP/Organoclay Nanocomposites

TG-DTA curves of PP and the nanocomposites are shown in Fig. 4.5 and Fig. 4.6. The temperature corresponding to initial dedradation temperature of weight loss (T_i), final degradation temperature of weight loss (T_f), the temperature at maximum rate of weight loss (T_d), and the char residue are given in Table 4.2. The TG-DTA curves show a single degradation step. It was observed that the degradation temperatures of the nanocomposites are higher than virgin PP and tend to increase with clay content. From the results, it can be concluded that the incorporation of clay in PP improves the thermal stability of the PP matrix and this improvement also increases with clay content. This behavior may be attributed to the formation of a high-performance carbonaceous-silicate char on the surface of the nanocomposites, creating a physical protective barrier on the surface of the material [3, 8].

Table 4.2 Thermal behavior of PP and PP/organoclay nanocomposites

Sample	TGA			
	Residue (wt%)	T_d (°C)	T_i (°C)	T_f (°C)
PP	-	443.7	420.5	453.7
PP/6%Surlyn/1%Clay	6.7	445.7	428.4	455.3
PP/6%Surlyn/3%Clay	7.1	446.6	427.0	456.1
PP/6%Surlyn/5%Clay	11.3	447.6	427.2	457.1

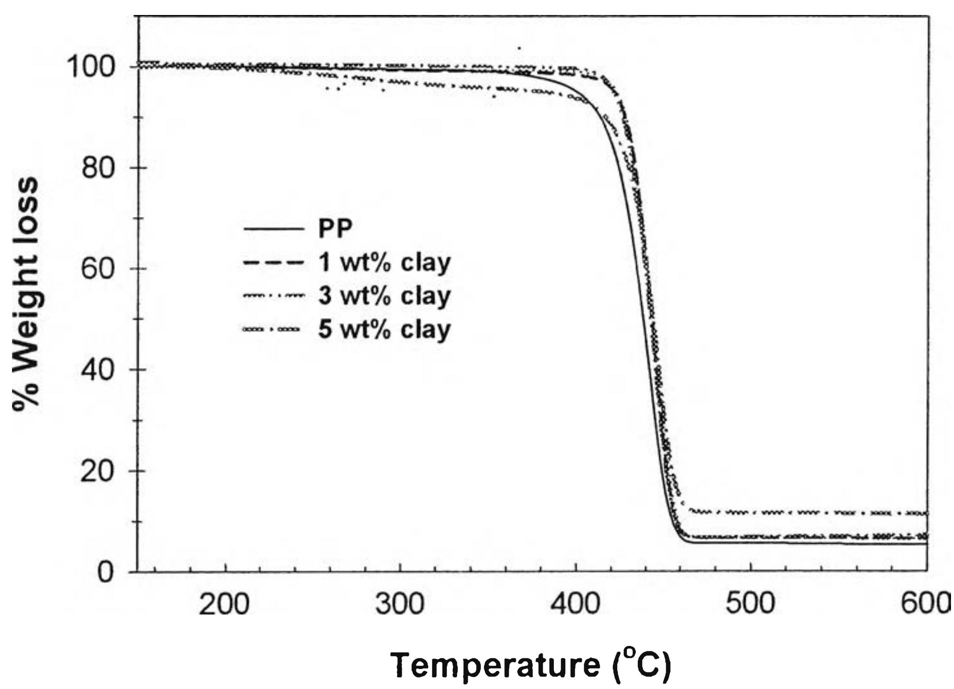

Figure 4.5 TGA thermograms of PP and PP/organoclay nanocomposites.

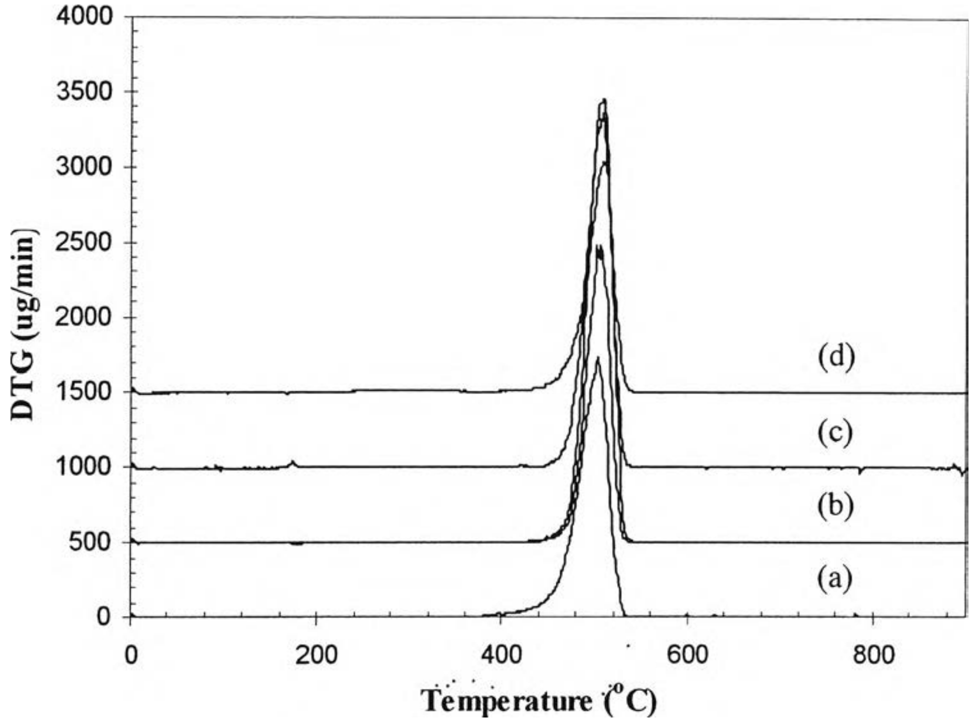

Figure 4.6 DTA thermograms of PP and PP/organoclay nanocomposites: (a) PP, (b) PP/6%Surlyn/1%Clay, (c) PP/6%Surlyn/3%Clay, and (d) PP/6%Surlyn/5%Clay.

D. Melting and Crystallization Behavior of PP/Organoclay Nanocomposites

The effects of clay content on melting and crystallization behavior of the nanocomposites was investigated by DSC. The peak values for melting (T_m) and crystallization temperature (T_c), as well as the melting enthalpy (ΔH_m) and %crystallinity for various clays content are listed in Table 4.4. The melting curves of the nanocomposites are presented in Fig. 4.7. It was observed that the melting temperature of the nanocomposites is greater than that of pure PP; however it is almost the same when the clay content is increased. As shown in Fig. 4.8, the crystallization temperature of the nanocomposites is shifted to higher temperature than that of virgin PP but less sensitive to the clay content (1, 3, 5 wt%). The crystallinities of the nanocomposites are slightly higher than that of pure PP. This could be attributed to the organo-modified clays acting as a nucleating agent for the crystallization of the PP matrix. However, the crystallinity of 5 wt% clay is lower than virgin PP. This may be due to the aggregation of organo-modified clay leading to the obstruction of the packing of the crystalline. From these results, the melting and crystallization temperatures of the nanocomposites are insignificantly changed by clay content. It can be concluded that the addition of clay has minimal effect on the melting and crystallization temperatures of the nanocomposites [9, 10].

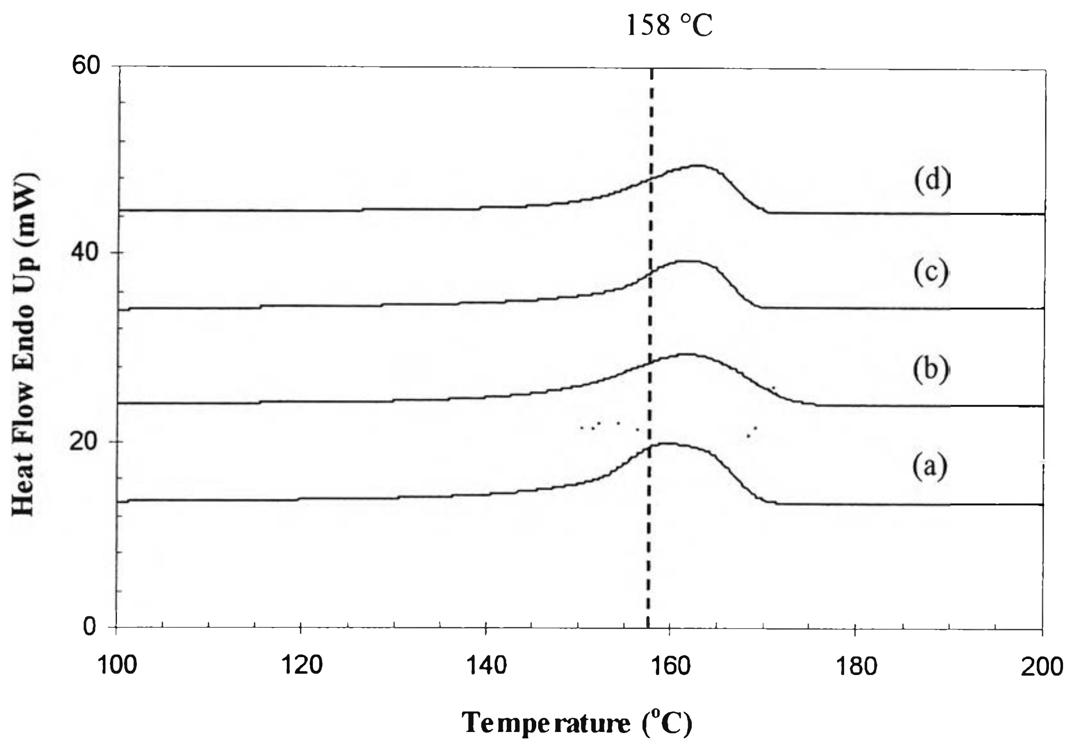

Figure 4.7 DSC thermograms (melting temperature) of PP/organoclay nanocomposites: (a) PP, (b) PP/6%Surlyn, (c) PP/6%Surlyn/1%Clay, (d) PP/6%Surlyn/3%Clay, and (e) PP/6%Surlyn/5%Clay.

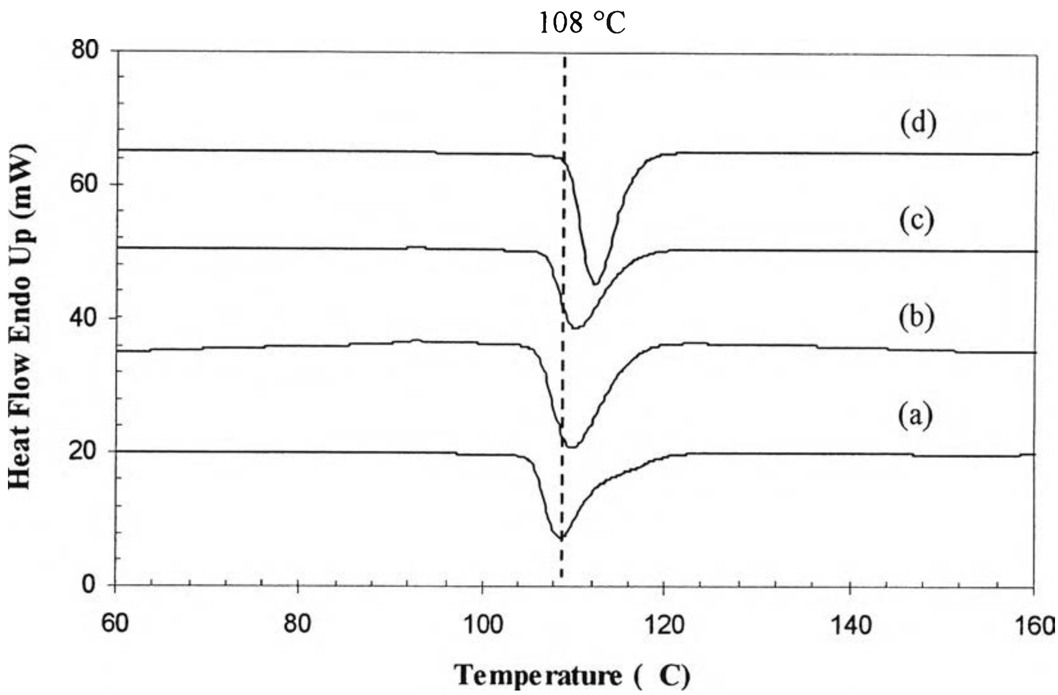

Figure 4.8 DSC thermograms (crystallization temperature) of PP/organoclay nanocomposites: (a) PP, (b) PP/6%Surlyn/1%Clay, (c) PP/6%Surlyn/3%Clay, and (d) PP/6%Surlyn/5%Clay.

Table 4.3 Melting and crystallization behavior of PP and PP/organoclay nanocomposites

Sample	**$T_{c,peak}$ (°C)**	**$T_{m,peak}$ (°C)**	**ΔH_m (J/g)**	**% crystallinity**
PP	108.63	158.37	69.46	33.23
PP/6%Surlyn/1%Clay	109.97	159.20	66.10	34.00
PP/6%Surlyn/3%Clay	110.30	158.87	64.61	33.97
PP/6%Surlyn/5%Clay	112.30	159.20	61.59	33.11

E. Mechanical Propertiest of PP/Organoclay Nanocomposites

The effect of clay contents on the mechanical properties, Young's modulus, tensile strength and elongation at break, of both PP and PP/organoclay nanocomposites are shown in Fig. 4.9, 4.10, and 4.11, respectively. The average values of these mechanical properties are reported in Table 4.4. PP and nanocomposite films have different thermal history. That is, nanocomposite films were prepared by using twin-screw extruder and blow molding whereas PP film was only processed by blow molding. Young's modulus of the nanocomposites was greater than that of pure PP. The Young's modulus was optimized at 1 wt%, and then gradually decreased when the clay content increases to 5 wt%. In case of tensile strength, it was lower than that of virgin PP and decreased with increasing the clay content. This may imply that the incorporation of clay into PP matrix reduced the ability of the composites to transfer applied stress. Moreover, the elongation at break of the nanocomposites was reduced with increasing the clay contents. The decrease in mechanical properties of the nanocomposites may involve with the aggregations of clay or the remaining of some impurities in bentonite. The aggregations of clays or the impurities in bentonite act as stress concentrators, allowing crack initiation and propagation, consequently decreasing mechanical performance of the nanocomposites [2].

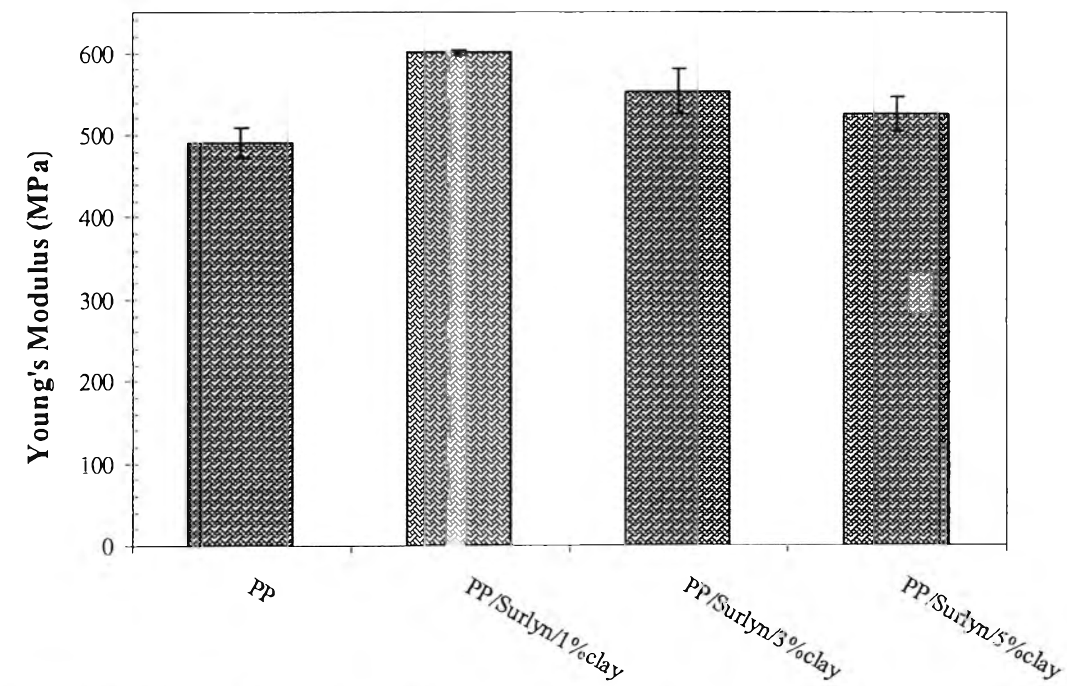

Figure 4.9 Young's modulus of PP and PP/organoclay composites

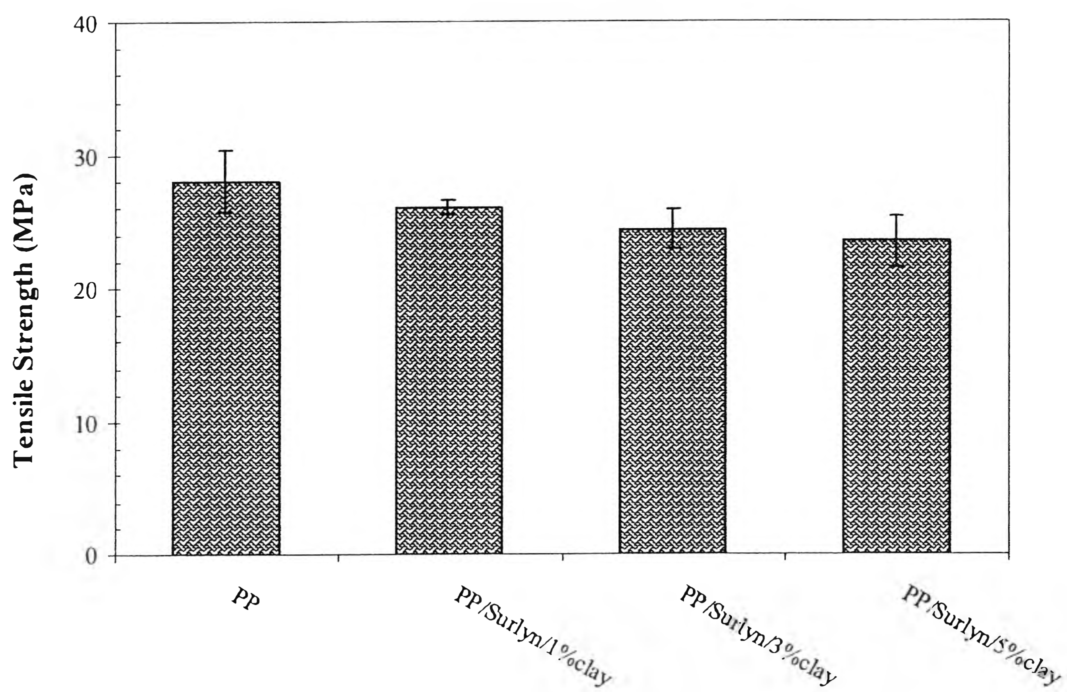

Figure 4.10 Tensile strength of PP and PP/organoclay composites

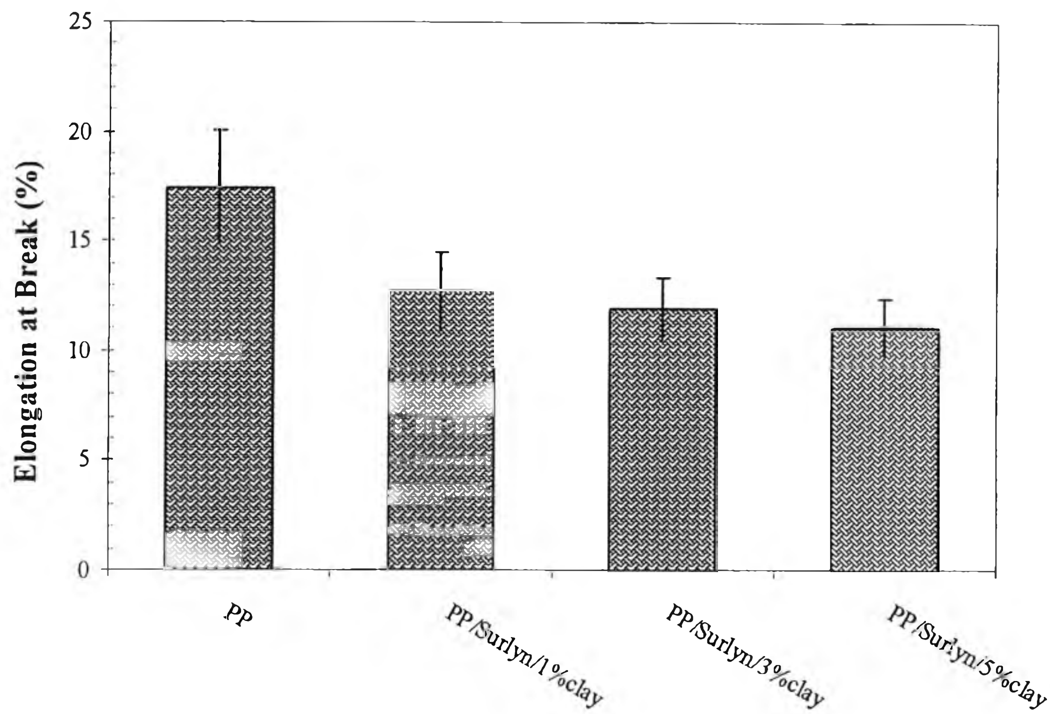

Figure 4.11 Elongation at break of PP and PP/organoclay composites

Table 4.4 Mechanical properties of PP and PP/organoclay nanocomposites

Sample	Young's Modulus (MPa)	Tensile Strength (MPa)	Elongation At break (%)
PP	491.53 ± 18.82	28.10 ± 2.31	17.44 ± 2.63
PP/6%Surlyn/1%Clay	600.89 ± 4.04	26.04 ± 0.55	12.73 ± 1.76
PP/6%Surlyn/3%Clay	553.18 ± 28.18	24.40 ± 1.48	11.92 ± 1.43
PP/6%Surlyn/5%Clay	524.95 ± 20.90	23.46 ± 1.85	11.08 ± 1.30

F. Dispersion of Organo-modified Clay in Nanocomposite Films

The dispersion of clay particles are better observed by scanning electron microscopy (SEM), as shown in Fig. 4.12. With increasing in clay contents, the agglomeration of silicate layers and the impurities in PP matrix could be formed that leads to poor compatible to the PP matrix. The effect of incompatibility between clay and PP matrix reduced mechanical properties in nanocomposites [11].

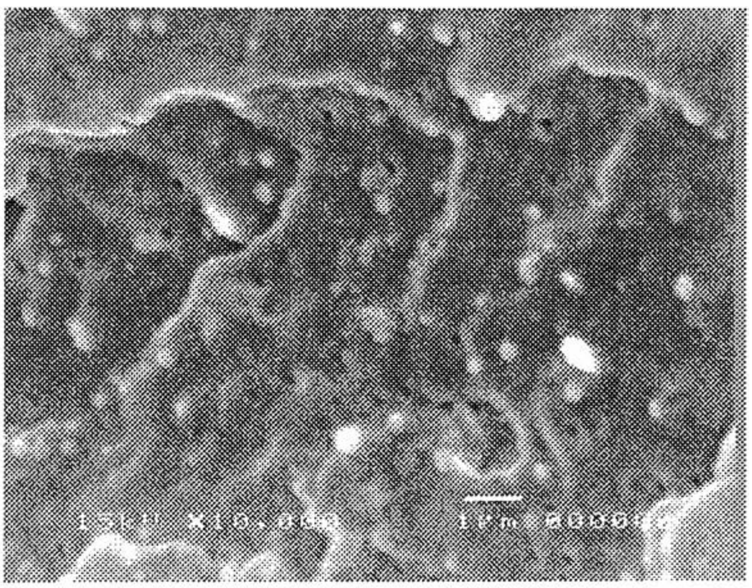

(a)

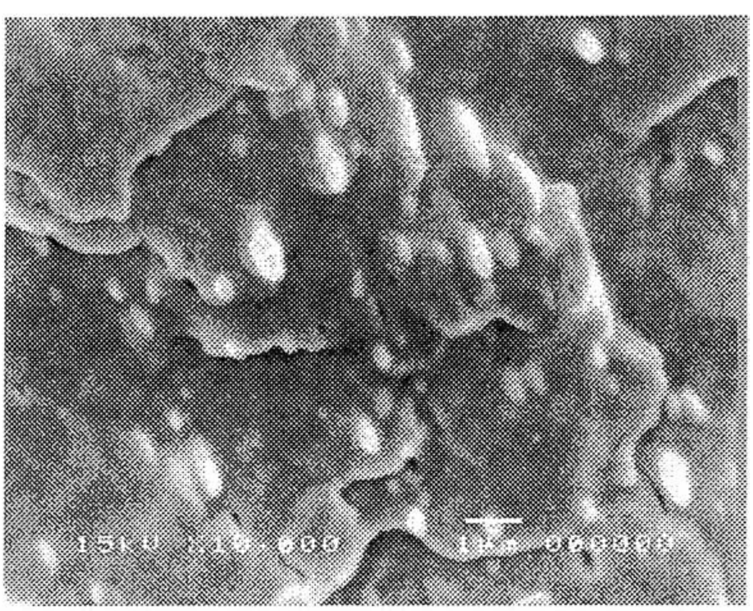

(b)

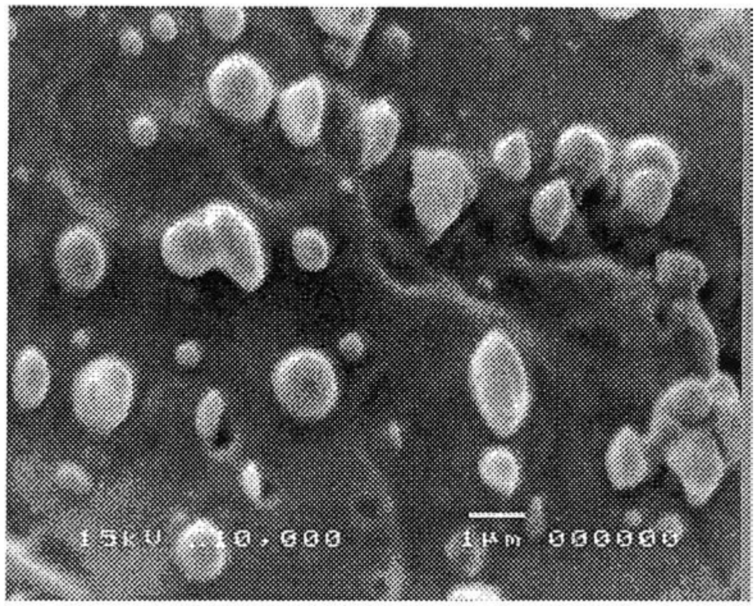

(c)

Figure 4.12 SEM images of PP/organoclay nanocomposites at 10000 magnify: (a) PP/6%Surlyn/1%Clay, (b) PP/6%Surlyn/3%Clay, and (c) PP/6%Surlyn/5%Clay.

G. Oxygen Permeability of PP/Organoclay Nanocomposite Films

The oxygen gas permeability of the nanocomposite films are shown in Fig. 4.13 and reported in table 4.5. Those films were the same film thickness of 150 μm. The oxygen gas permeability of the nanocomposite films was lower than that of pure PP and reduced slightly with increasing the clay content. The reduction of oxygen gas permeability can be attributed to more tortuous path that retard the progress of gas molecules through the PP matrix, providing the improvement of gas barrier properties [12]. Another possible explanation for the reduction in permeability is that crystalline act in a similar manner to crosslinking, restricting the motion of the chains involved in the diffusion process [13].

Table 4.5 Oxygen Gas Permeability of PP and PP/organoclay nanocomposite films

Sample	Oxygen Gas Permeability ($cc/m^2.day$)
PP	3580 ± 84
PP/6%Surlyn	1649 ± 139
PP/6%Surlyn/1%Clay	634 ± 19
PP/6%Surlyn/3%Clay	627 ± 16
PP/6%Surlyn/5%Clay	615 ± 40

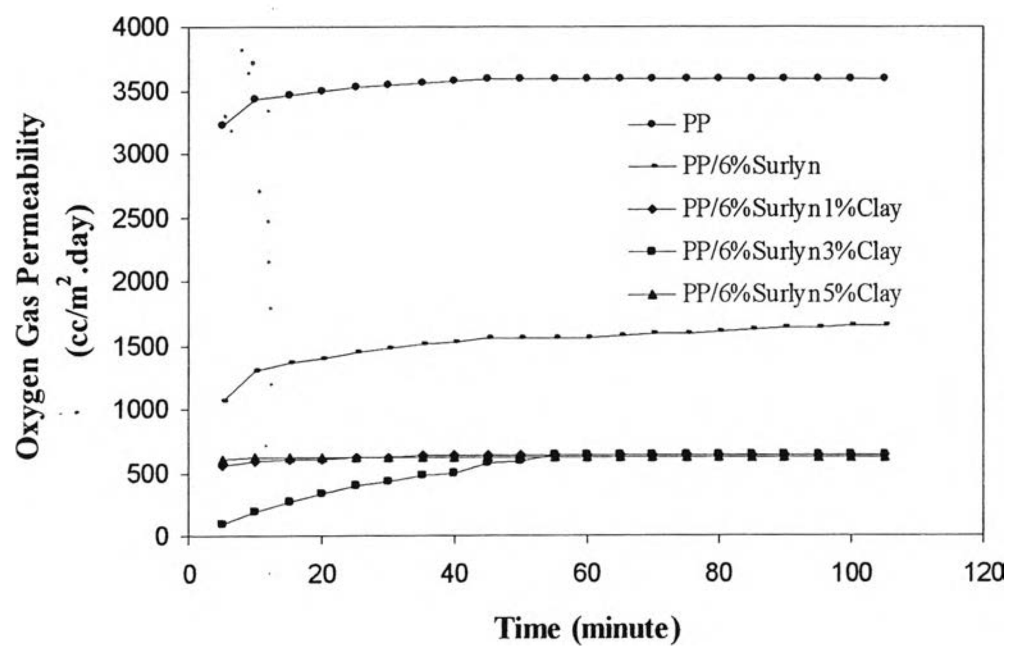

Figure 4.13 Oxygen Gas Permeability of PP and PP/organoclay nanocomposite films

From XRD and oxygen permeability results, it could be assumed that some exfoliated structure was achieved in this experiment. However, the mechanical properties were reduced which may involve with the aggregation of clays and the impurities. This gives contrast result with XRD and oxygen permeability. It may be implied that some aggregation would be associated with the exfoliation of silicate layers.

4.5 Conclusions

The properties of PP/organoclay nanocomposites, crystal structure, thermal behavior, mechanical properties and oxygen gas permeability, were studied and compared to pure PP. According to XRD patterns, the addition of the organoclay does not affect the crystal structure of PP matrix. However, the incorporation of the organoclays can enhance the thermal stability of PP/organoclay nanocomposites. The melting and crystallization temperatures of the nanocomposites are higher than those of pure PP but less sensitive to the clay content. It can be concluded that the addition of clay has minimal effect on the melting and crystallization temperatures of the nanocomposites. The crystallinities of the nanocomposites are slightly higher than that of pure PP. This could be attributed to the organo-modified clays acting as a nucleating agent for the crystallization of the PP matrix. Young's modulus of the nanocomposites was greater than those of pure PP and gradually decreased when the organoclay content increases to 5 wt%. In case of tensile strength, it was lower than that of virgin PP and decreased with increasing the clay content. Moreover, the elongation at break of the nanocomposites was reduced with increasing the clay contents. The decrease in mechanical properties of the nanocomposites may involve with the aggregations of clay or the remaining of some impurities in bentonite. The oxygen gas permeability of the nanocomposite films was lower than that of pure PP and reduced slightly with increasing the clay content.

4.6 Acknowledgements

This work is funded by the National Research Council of Thailand (NCRT), Polymer Processing and Polymer Nanomaterials Research Units and National Excellent Center for Petroleum, Petrochemicals, and Advanced Materials, Thailand. The authors would like to thank Thai Nippon Chemical Industry Co, Ltd., for providing the raw materials to carry out this research and Tang Packaging Co., Ltd. for tubular blown film extrusion machine.

4.7 References

1 Ray, S.S. and Okamoto, M. (2003) Progress in Polymer Science, 28, 1539-1641.

2 Garcia-Lopez, D., Picazo, O., Merino, J.C., and Pastor, J.M. (2003) European Polymer Journal, 39, 945-950.

3 Ramos, F.G., Melo, T.A., Rabello M.S., and Silva, S.M. (2005) Polymer Degradation and Stability, 89, 383-392.

4 Choy, J., Kwak, S., Han, Y., and Kim, B. (1997) Materials Letters, 33, 143-147.

5 Ding, C., Jia, D., He, H., Guo, B., and Hong, H. (2004) Polymer Testing, 24, 94-100.

6 He, H., Duchet, J., Galy, J., and Gerard, J-F. (2005) Journal of Colloid and Interface Science, 288, 171-176.

7 Lai, S., Chen, J., and Chu, P. (2004) Polymer Science, 42, 4139-4150.

8 Modesti, M., Lorenzetti, A., Bon, D., and Besco, S. (2006) Polymer Degradation and Stability, 91, 672-680.

9 He, J.D., Cheung, M.K., Yang, M.S., Qi, Z. (2003) Journal of Applied Polymer Science, 89, 3404-3415.

10 Wang, D., Xu, D., Zhang, X., Yang, M., Dong, X. (2004) Journal of Applied Polymer Science, 92, 552-558.

11 Szazdi, L., Pkanszky, B., Vancso, G.J.; and Pukanszky, B. (2006) Polymer, 47, 4638-4648.

12 Di, Y., Lannac, S., Sanguigno, L., and Nicolais, L. (2005) Macromol. Symp., 228, 115-124.

13 Wang, Y., Easteal A.J., and Chen, X.D. (1998) Packaging Technology and Science, 11, 169-178.